APPLICATION OF ANOMALOUS WAVE PROPAGATION IMAGING METHOD WITH ADJACENT WAVE SUBTRACTION TO ACTUAL DAMAGES IN COMPOSITE WING

Chen Ciang Chia[1], Jung-Ryul Lee[1]*, Chan-Yik Park[2]
[1] Department of Aerospace Engineering, Chonbuk National University, Jeonju, Chonbuk, Republic of Korea, [2] Aeronautical Technology Directorate, Agency for Defense Development, Daejeon, Republic of Korea
* Corresponding author (leejrr@jbnu.ac.kr)

Keywords: *field-test, laser ultrasonics, nondestructive evaluation, debonding, impact damage*

Abstract
Anomalous wave propagation imaging method was applied for the on-site in-situ nondestructive evaluation of actual debonding and impact damages in a composite wing with high density of structural elements. The promising results showed that it has high potential as on-site nondestructive evaluation method of other complex engineering structures.

1 Introduction

Structural health monitoring (SHM) and nondestructive evaluation (NDE) technologies can accrue enormous economic and life-safety benefits. Among the many schemes adopted in these technologies, the guided acousto-ultrasonic wave technique is one of the widely accepted schemes. Based on the laser ultrasonic scheme, we developed the anomalous wave propagation imaging (AWPI) method with adjacent wave subtraction, and the Variable Time Window Amplitude Mapping (VTWAM) in our previous work [1]. The results from laboratory tests were compared favorably with the results of an immersion ultrasonic C-scan. However, application to aerospace structures is not straightforward due to the stringent requirements imposed by the regulatory agencies. Extensive laboratory investigations are required, and validation in actual structures for the evaluation of real damage is emphasized. The field application of the AWPI method in this study was conducted in the endeavor of seeking wider acceptance of this method by the aerospace industry. It was conducted using a newly proposed test setup with a built-in laser ultrasonic propagation imaging system [2] that can be expanded easily for automatic laser-based NDE of wing structures in a whole hanger.

2 Field Application of the AWPI Method

2.1 Core Components and Setup

The hardware needed for the application of the AWPI method is the ultrasonic propagation imaging system [2]. A laser ultrasonic generator produces laser pulses, a galvanometric laser mirror scanner deflects the laser pulses toward the inspection structure for ultrasonic wave generation, and the ultrasonic receiver integrated in the structure captures the ultrasonic waves for result processing. The laser adopted in this study was a Q-switched Nd:YAG diode-pumped solid state laser (QL). Its wavelength, diameter of the laser beam at the exit port of the laser head, divergence, and pulse duration was 532 nm, 0.7 mm, 1.6 mrad, and 30 ns, respectively. In practice, the 532 nm visible green laser beam provides convenience when an inspector controls the scanning area. The ultrasonic receiver selected for this study was an omni-directional, amplifier-integrated broadband piezoelectric sensor with a cut-off frequency of 2 MHz and diameter of 4 mm.
The target of inspection in this study was a real wing testbed of an unmanned aerial vehicle, attached to an H-beam fixture shown in Fig. 1. The testbed was made of carbon fiber reinforced plastic, with common wing structural elements such as spars, stringers, ribs, and skin. Both the laser and the scanner were put on a two-axis slider above the testbed, and the rest of the system components not related to laser scanning were installed in a mobile rack on the ground level. The two-axis slider could be easily repositioned to facilitate inspection at an arbitrary site. Using this configuration, the laser pulses could be deflected by the scanner towards the

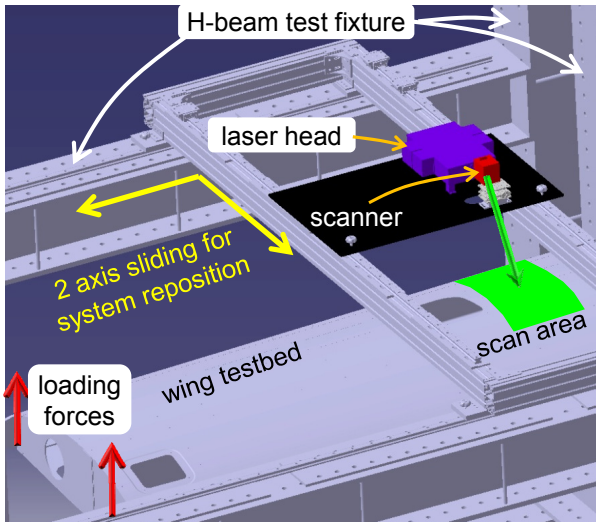

Fig. 1. Field test setup for real wing inspection.

scanning grid points on the upper surface of the testbed easily. Optimum scanning grid with a pitch of Δ=1.0 mm and a laser pulse repetition frequency of 1 kHz were used throughout this study after considering the inspection speed, the resolution of the results, and the reverberation effect. All signals were sampled using 500 data points.

2.2 Algorithms

Algorithms tested in this study were the AWPI and the VTWAM. The AWPI can enhance the visibility of the anomalous waves, which finally works as an enhanced damage evaluation algorithm for the ultrasonic propagation imaging system. In this context, the anomalous waves are the waves related to the structural anomalies, including the scattering waves and the confining waves. The AWPI was developed based on the feature that the time domain ultrasonic signals acquired from two adjacent laser scanning grid points are highly similar. Subtraction of the adjacent wave hence suppresses the incident waves and exaggerates the anomalous waves. The VTWAM was developed based on the time difference of the incident waves and the anomalous waves. The anomalous wave appears after the incident wave sweeps over the structural anomaly, and the confining wave with features similar to the standing wave exhibits a longer duration time within the damage. Using the VTWAM after the AWPI processing can generate an amplitude map that shows the location, size, and shape of the damages resemble to the actual damages.

3 Field Inspections

3.1 Case I: Suitability for Smart Structures

Case I was conducted to show the suitability of the AWPI for the inspection of smart structures with integrated transducers. Hence, the testbed was inspected when it was in intact condition, and the inspection area was selected to include three 18 mm PZT (lead zirconate titanate) elements bonded between the stringers, as shown in Fig. 2. These PZT elements did not participated in the waves sensing, but were merely a type of material discontinuity in this study. The ultrasonic sensor used for this inspection was temporarily bonded on the internal surface of the wing skin at the position shown in Fig. 2. The size of the inspection area, the fluence of the QL, the bandpass, and the sampling time interval were set to 300×300 mm^2, 37 mJ/cm^2, 240-290 kHz, and T=0.4 μs, respectively.

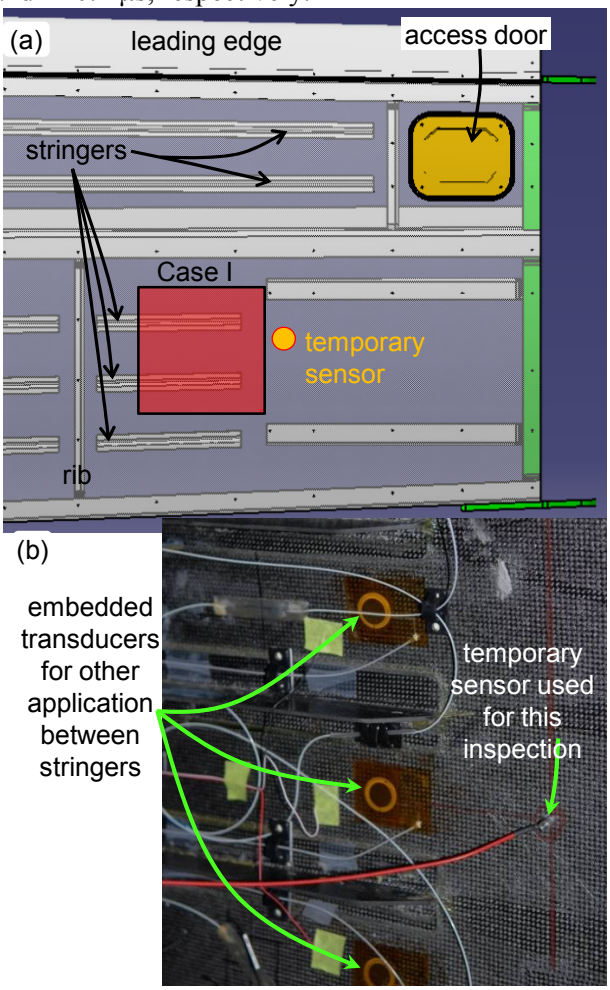

Fig. 2. Inspection Case I. (a) Inspection area. (b) Internal view of the wing testbed.

3.2 Case II: Evaluation of Debonding Damages

Case II was conducted after the wing underwent a series of destructive bending tests. The inspection area was selected at a damage hot spot, as shown in Fig. 3. This inspection area was selected because it contained many other structural elements including the boundary of the inspection window, rib flange, and the lug, and an integrated ultrasonic sensor (IS1) was available at the spar web. It was selected intentionally to show that the high density of structural elements would not interfere with the normal AWPI inspection. The size of the inspection area, the fluence of the QL, the bandpass frequency, and the sampling time interval were set to 200×200 mm^2, 34 mJ/cm^2, 60-200 kHz, and T=0.6 μs, respectively.

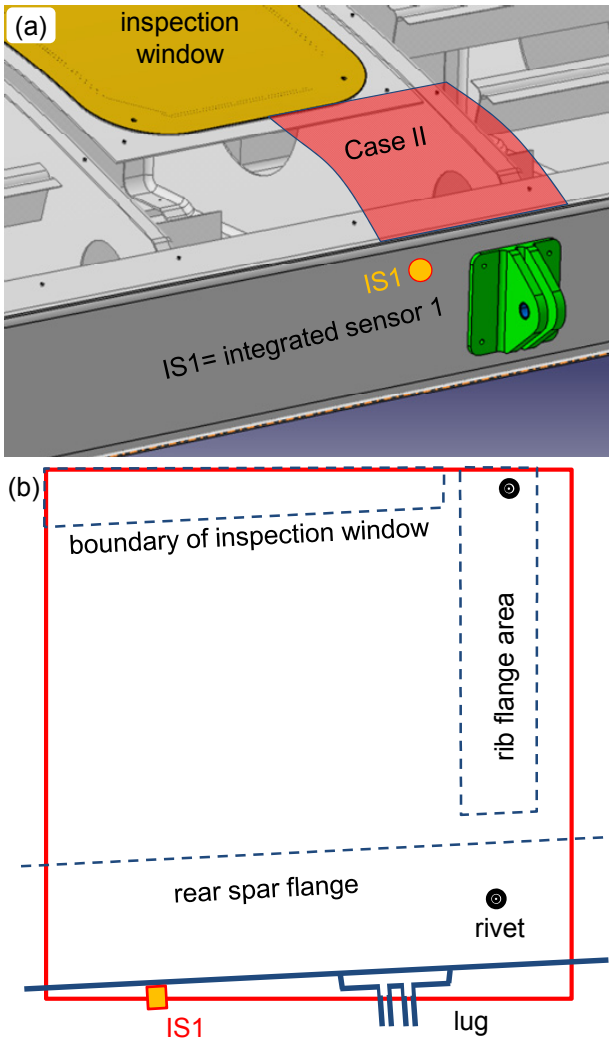

Fig. 3. Inspection Case II. (a), (b) high density of structural elements within the inspection area.

3.3 Case III: Evaluation of Impact Damages

The testbed was impacted in order to find the critical impact energy of the testbed, and to show the capability of the developed AWPI method for real impact damage evaluation. The impact site was selected near one of the most complex areas of the testbed, as shown in Fig. 4. Three impact events tabulated in Table 1 were made between the rib and stringers using an indenter of 4 mm diameter. Two integrated sensors were available for the inspection of the impact damages. The IS2 and IS3 were integrated at the web of the rib, 30 mm from the upper skin, as shown in Fig. 4. The redundancy of the sensor within a small region of the wing was designed to crosscheck the results obtained from two sensors. The size of the inspection area, the fluence of the QL, the bandpass filtering, and the sampling time interval were set to 300×300 mm^2, 75 mJ/cm^2, 60-200 kHz, and T=0.8 μs, respectively.

Table 1. Details of impact events.

Event	Energy	Visual inspection
E1	15 J	Invisible
E2	15 J	Invisible
E3	25 J	13 mm diameter puncture

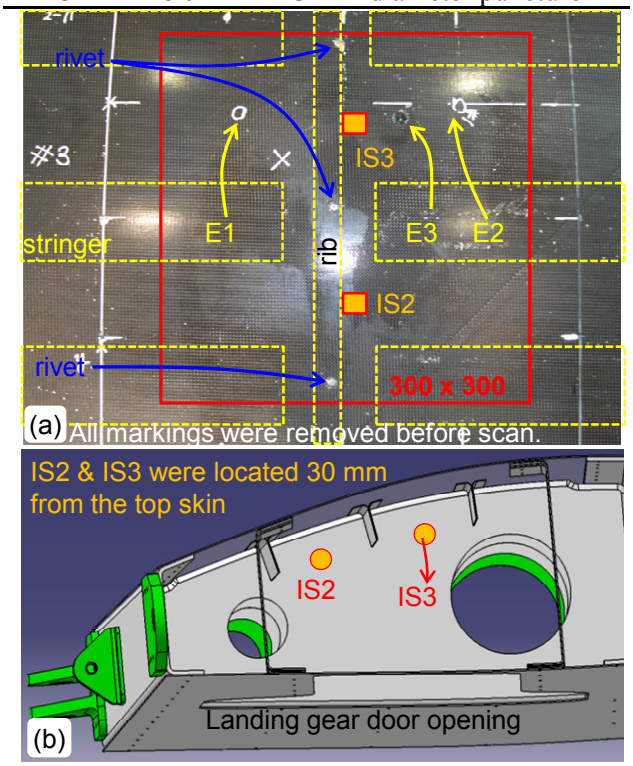

Fig. 4. Inspection Case III.

4 Results and Discussions

4.1 Case I: Suitability for Smart Structures

The freeze-frames of the AWPI movie at 74 and 114 μs are given in Figs. 5(a) and (b), respectively. The residual of the incident wave is shown as if emanating from the signal sensing point, and its encounter with the stringer tips generated scattering waves as shown in Fig. 5(a). Its encounter with the bare PZT elements as added masses generated another scattering wavefields, as shown in Fig. 5(b). The freeze-frames show no occurrence of confining wave within the PZT transducers. In other words, they were detected as simple structural discontinuities. This was an encouraging result because it suggests that the AWPI method can be used for structures with integrated PZT elements. No confining wave is shown in the freeze-frame after the residual of the incident wave swept through the area of inspection. This result also proves that the system works well in the field environment.

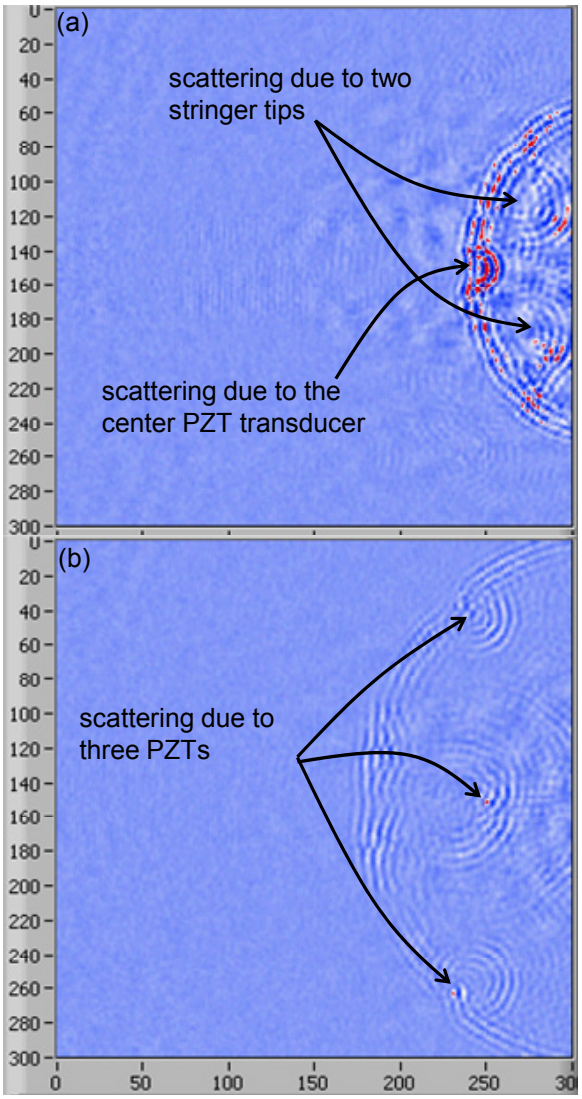

Fig. 5. Freeze-frames of the AWPI movie at (a) 74, and (b) 114 μs showing no confining waves in PZTs.

4.2 Case II: Evaluation of Debonding Damages

The freeze-frame of the AWPI movie at wave propagation time of 120 μs is given in Fig. 6(a). It shows the anomalous wave at the bottom left. A part of the anomalous wave with higher amplitude was due to the direct impingement of the laser on the IS1 and the lead wire used for this inspection. Also shown in this freeze-frame are the confining wave for a small damage and the silhouette of the lug. The VTWAM in Fig. 6(b) shows clearly two damage events (with bright colors), corresponding to the rear spar-skin debonding. The high amplitude due to the sensor and the lead wire is shown in red, and the high amplitude due to a part of the lug is also shown. These results show that the AWPI combined with the VTWAM method is effective in evaluating the debonding damages, and the boundary of the inspection window, rib flange, and lug would not adversely affect the inspection.

4.3 Case III: Evaluation of Impact Damages

For inspection using IS2, the freeze-frame of the AWPI movie at wave propagation time 168 μs is given in Fig. 7(a). It shows the confining anomalous waves at the edges of the stringers and the impact location E1, which implies damages there. The VTWAM is shown in Fig. 7(b) with the outlines of the internal structural elements. The VTWAM show two damages related to impact E1 and E3, but no sign of damage for impact E2. In addition to the impact damages, it reveals the debonding in the stringer edges in the wing tip direction. Since the damages in the stringer tip were not found in inspection Case I before structural loading tests, it provides strong evidence that the upward bending of the testbed at the wing tip generated debonding at the stringer tips. In fact, this type of damage is notorious in the stiffened panels widely used in the aerospace industry. Three more areas with high amplitudes are shown in the VTWAM at the side boundaries of the stringers. We believe that stringer-skin debonding also occurred at these locations.

For the crosscheck based on IS3, the freeze-frame of

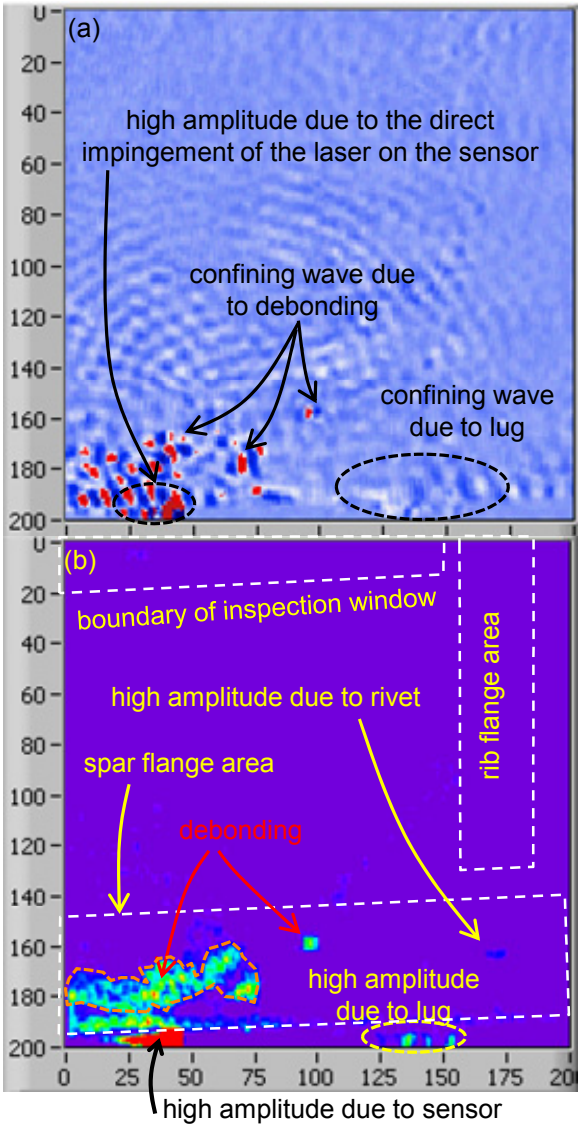

Fig. 6. Results of Case II. (a) Freeze-frame of AWPI movie, (b) VTWAM showing two debonding.

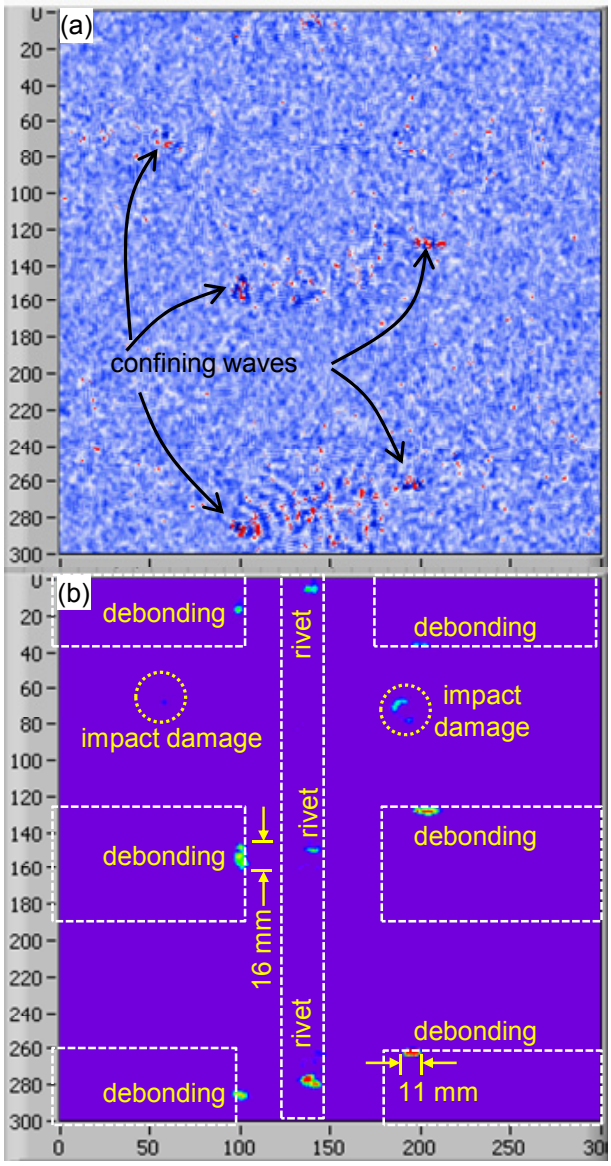

Fig. 7. Results of Case III using IS2. (a) Freeze-frame of AWPI movie, (b) VTWAM image.

the AWPI movie at wave propagation time 220 μs is given in Fig. 8(a). Similar to the inspection based on IS2, the confining anomalous waves are also shown in the freeze-frame at the edges of the stringers and the location of impact E1 and E2. For better damage evaluation, the VTWAM was generated and shown in Fig. 8(b). Comparison of Fig. 7(b) and Fig. 8(b) shows good agreement in the damage size evaluation. The size of the damages varied between 7 and 11 mm for the damage with greatest size deviation, while between 16 and 17 mm for the damage with smallest size deviation. These two VTWAMs show the presence and location of the damages consistently, which proved that the inspection is almost independent of the sensor position.

4.4 Other Findings

The results showed the rear spar-skin debonding damages between two riveted locations, indicating skin buckling during the wing bending. Also, stringer debonding due to wing bending occurred at all stringer tips in the wing tip direction, which agreed well with the notorious stringer tip debonding damage commonly found in aerospace structures.

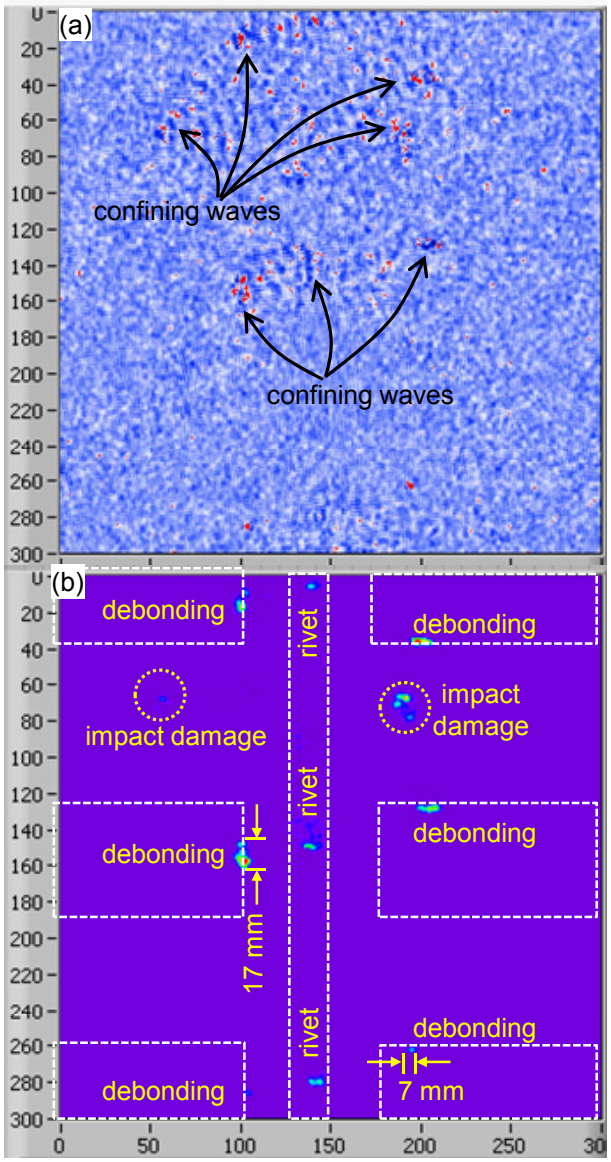

Fig. 8. Results of Case III using IS3. (a) Freeze-frame of AWPI movie, (b) VTWAM image.

Furthermore, it can be deduced that the critical impact energy for the testbed was 15 J. This is because the results of Case III based on IS2 and IS3 showed that only impact E1 damaged the wing testbed despite both the impact E1 and E2 were 15 J. The presence of structural elements or features such as spars, stringers, ribs, lugs, inspection windows, and even surface mounted PZT elements did not adversely affect the inspection process. This proved the suitability of the method for the NDE of complex engineering structures. Lastly, the robustness of the system for on-site application is self-explanatory because all inspection were conducted successfully using the same equipments as in the laboratory test without additional modification.

5 Conclusions

Anomalous wave propagation imaging (AWPI) method with adjacent wave subtraction and Variable Time Window Amplitude Mapping (VTWAM) were tested in the field environment for the nondestructive evaluation of a real wing that underwent bending and impact loadings. The tests were conducted using a newly proposed test setup that can be expanded easily for automatic laser-based NDE of wing structures in a whole hanger. The inspection results proved that the system works well for on-site in-situ evaluation of real debonding and impact damages, including stringer tip debonding, skin-spar debonding, and invisible impact damage. The presence of structural elements or features such as spars, stringers, ribs, lugs, inspection windows, and even surface mounted PZT elements did not adversely affect the inspection process. These results prove that the AWPI method combined with the VTWAM is effective, and it has high potential as an on-site NDE method for other complex engineering structures.

Acknowledgement

We performed this study under the applied research project (UC080019JD) which is supported by ADD (Agency for Defense Development) in Korea. This work was also supported by the National Research Foundation of Korea (NRF) grant (2011-0010489) funded by the Korea government (MEST) and by Korea Ministry of Land, Transport and Maritime Affairs as Haneul Project.

References

[1] J.-R. Lee, C. C. Chia, C.-Y. Park, H. Jeong. “Laser ultrasonic anomalous wave propagation imaging method with adjacent wave subtraction: algorithm”. (submitted to *Opt. Laser Technol.*, 2011)

[2] J.-R. Lee, H. Jeong, C. C. Chia, D.-J. Yoon, and S.-S. Lee. “Application of ultrasonic wave propagation imaging method to automatic damage visualization of nuclear power plant pipeline”. *Nucl. Eng. Des.*, Vol. 240, pp 3513-20, 2010.